

Forward and inversion modelling of the ultrasonic wave in a homogeneous medium using P-wave transducers

Michel M. Nzikou^{1*}
Curtin University
Exploration Geophysics
Perth, WA

Alexey Yurikov²
Curtin University
Exploration Geophysics
Perth, WA

Mahyar Madadi³
Curtin University
Exploration Geophysics
Perth, WA

Maxim Lebedev⁴
Curtin University
Exploration Geophysics
Perth, WA

Boris Gurevich⁵
Curtin University
Exploration Geophysics
Perth, WA

¹michel.nzikouma@postgrad.curtin.edu.au ²Alexey.yurikov@postgrad.curtin.edu.au ³Mahyar.Madadi@curtin.edu

⁴M.Lebedev@curtin.edu.au ⁵B.Gurevich@curtin.edu.au

*presenting author asterisked

SUMMARY

We use full wave forward and inversion modelling to estimate the elastic properties of rock samples from ultrasonic waveforms. The finite element algorithm (ABAQUS modelling software) is used to model a forward wave propagation within a homogeneous medium. For 19 mm diameter P-wave transducers, the result of the displacement waveform for a uniform source signal is obtained using both a linear and radial (about 2 mm) receiver arrays. Also, the use of a non-uniform source amplitude such as Gaussian distribution improves the displacement waveforms by few percent. The results accuracy is increased with increasing values of Gaussian standard deviation. However, for a nominal frequency of 1MHz, the same error increases with the decreasing frequencies. Additionally, our inversion algorithm (written in Python) searches for the best Young modulus (E) and Poisson ratio (ν) of the medium iteratively. Finally, without prior knowledge of any threshold, the elastic parameters are estimated, and the results are consistent with the experimental measurements. These results provide a new modelling workflow to estimate the elastic parameters of the homogeneous and isotropic sample.

Key words: Forward, inversion, Abaqus modelling, linear and radial arrays.

INTRODUCTION

Ultrasonic measurements are the main methods for measuring the rock elastic properties. In these methods, the elastic parameters are estimated from traveltimes obtained using traditional methods such as travel time picking and cross-correlation algorithms. These methods can produce errors in presence of distorted signal due to attenuation and dispersion, and the finite size transducers and their complex radiation pattern. In addition, other factors that can complicate the identification of the elastic parameters are obscuring waves such as side reflections. Therefore, without prior knowledge of these factors, the modelled elastic parameters can be erroneous and be interpreted wrongly.

The full waveforms modelling and inversion can overcome some of these problems. These methods can help to understand the nature of all the arrivals and also can correct the systematic errors introduced by the finite size transducers observed in ultrasonic data. Moreover, we can match the wave train, and then invert for both P and S using one piezoelectric (PZT) transducer (Olympus, 2007). A number of authors have estimated the elastic parameters of cylindrical sample using the first break travel time and phase velocity methods (Simons, 1987; Vernik, 1994; Lee and Waite, 2009; Chen et. al., 2014; Shragge, J. et. al., 2015; Yoshimitsu et. al., 2016; Akram and Eaton, 2016). Dellinger and Vernik (1994) assume an amplitude threshold of 1% to pick the first break arrival time. This assumption can be erroneous in presence of intergranular contacts and pore-space (Yun et. al., 2006, Santamarina, et. al., 2001), strong boundary reflection (Rasolofosaon and Zinszner, 2014, Yoshimitsu et. al., 2016), and dispersion (Mikhaltsevitch et.al., 2014; Qi et. al., 2015). Moreover, due to uncertainty of the source signal, there are still many challenges to match the waveforms accurately. Alles et. al., (2010) show that the transducer sizes and geometrical configuration has to be accounted to ensure the accuracy of the modelling (Daley and Hron, 1977). Lee and Waite (2009) show that the first arrivals depend on the sample geometry and cannot be estimated

from the waveforms easily. Therefore, a robust estimate of the elastic parameters requires an understanding of source/sample parameters and geometry.

One way to recover the elastic parameters is to use full-wave inversion (FWI). This approach can be very challenging due to the properties of various layers in the subsurface. Shragge et. al. (2015) simulated the elastic velocity of cylindrical samples observed in ultrasonic laboratory data, and also developed a 2D ultrasonic inversion workflow to image fracture in Poly methyl methacrylate (PMMA) sample. However, it is possible to invert the elastic velocity of 3D laboratory sample. Elastic parameters as well as the attenuation estimations could be affected by the transducer contacts between another surface or by the nature of complex radiation patterns due to finite size transducers in ultrasonic frequencies. In this work, a forward model and inversion algorithm is built to estimate the elastic parameters that improve the fidelity of the displacement waveforms using various source functions. We model the effect of the transducer misalignment that enhances our data acquisition, also discuss the importance of the amplitude distribution of the source, and finally invert the data for the elastic parameters using two type of source/receivers arrays.

1- EXPERIMENTAL MEASUREMENTS

The waveforms in cylindrical aluminium (AL) sample with density 2697.8 kg/m^3 and physical dimensions $77.48 \times 38.4 \text{ (mm)}$ (*length x diameter*) were acquired using a 19 mm diameter (0.75 inches) disk-shaped P-wave transducer with a central frequency of 1 MHz . The ratio of the sample-thickness to transducer-diameter is greater than 4 and it is in accordance with the standard sample transducer ratio (Dellinger and Vernik, 1994). Our modeling hypothesis state that a misalignment of up to the order of P-wavelength cannot affect the displacement waveforms (To be discussed later). Therefore, one can acquire the data for a voltage pulse of 100 V with much flexibility. We measure the transducer surface displacement as well as the axial displacement waveforms in AL sample for a total time of $30 \mu\text{s}$.

2- RESULTS AND DISCUSSIONS

1. FORWARD MODELLING

The waveforms are numerically obtained using Abaqus finite element analysis software through its explicit solver module. To reach a stable solution, the following parameters were used: grid size $\Delta x = \Delta y = \Delta z = 0.00045 \text{ m}$ (0.45 mm), density $\rho = 2700 \text{ kg/m}^3$, $E = 69 \text{ GPa}$, and $\nu = 0.35$. Note that, the displacement waveforms are recorded along the sample rotational axis. In this section, we show the results of the modelling of the axial displacement waveforms and discuss the possible effect that could originate the misfit of the wave train.

Figure 1 shows various frames of the wave propagation in AL sample view from source and receiver sides. For a uniform input amplitude, we show a good agreement of P-wave first break arrival time $T_6 = 15.12 \mu\text{s}$ (Circular white spot). T_6 can be used to calibrate results of correlation methods and also used as a model guess for inversion.

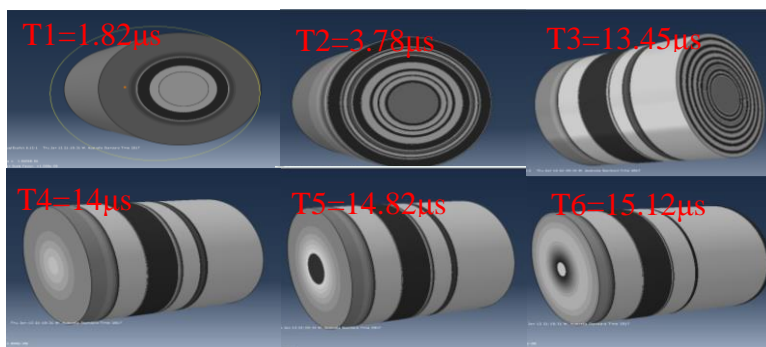


Figure 1: Wave propagation at different time intervals. $T_1 = 1.82 \mu\text{s}$ view from the source and $T_6 = 15.12 \mu\text{s}$, a record of P-wave first break arrival.

In Figure 2, seven waveforms consisting of various transducer shifts ($0, 0.75, 1, 2, 3, 4, 9.525 \text{ (mm)}$) (black colour) compared with the experimental data (red colour) are shown. The central shift or 0 mm shift is shown by the bottom black trace. The result of P-wave amplitude matches very well for the entire shifts. However, there is a visual difference after P-wave envelope. Besides the apparent broadening of the waveform amplitude for the far shifts, the overall average does not show any significant variations of waveforms

features. The broadening of waveforms for far offset could be due to the strong effect of the boundaries after the observed P-wave (Li et. al., 2000).

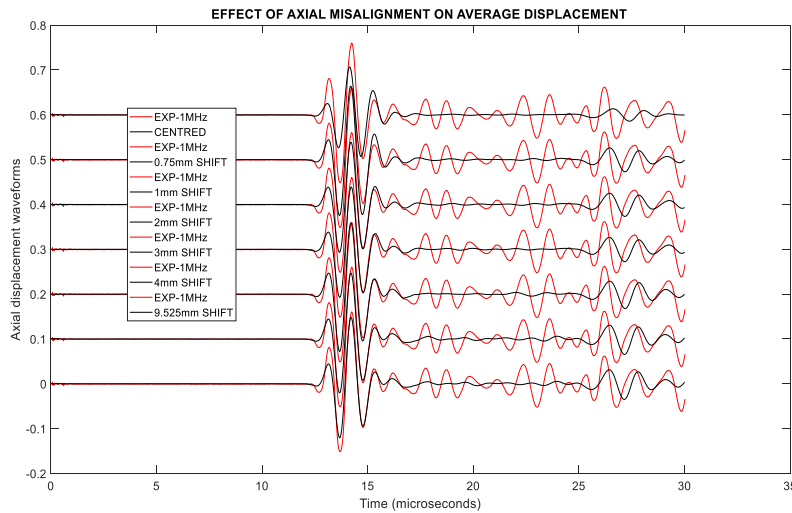


Figure 2: Measured (red) and average synthetic axial displacement waveform modelling in AL sample using uniform source input for a linear array transducer/receiver. Both transducers are shifted from the centre to the edge of the sample. From bottom to top, black curves represent shifted waveforms in this order 0, 0.75, 1, 2, 3, 4, 9.525 (mm).

The relative percentage difference (% diff) between the synthetic and experimental data is given by 1.157, 1.168, 1.175, 1.188, 1.228, 1.254, 1.483 corresponding to the shifts 0, 0.75, 1, 2, 3, 4, 9.525 (mm), respectively. The error in this model increase with the increasing shift. For a minimum wavelength of about 6 mm, the overall deviation in % diff even for larger shift such as 9.525mm is about 0.12. This may suggest that the waveform is not affected by the shift of less than the medium P- wavelength. This could possibly due to the less evasive effect of the boundary reflections recorded at the far offset (nodes). A low error provided confidence for our experimental data acquisition.

Besides, few effects such as signal distortion and the transducers finite size, the misfit showed in Figure 2 might be due to the uncertainty of the source input distribution or the model grid size. In Figure 3, the measured (red) and average synthetic waveforms in AL sample being shown. Visually, a Gaussian distribution improves the accuracy of the wave train. The measure of their goodness of fit (GOF) for 25%, 50% and 75% are 0.2587, 0.4051 and 0.4272, and also, their % diff are 1.359, 1.1172, and 1.0870, respectively. The error produced with the amplitude broadening decreases with the increasing σ , with higher accuracy obtained for $\sigma = 75\%$. This could suggest that the magnitude of the source input amplitude does not fluctuate much from the transducer centre displacement.

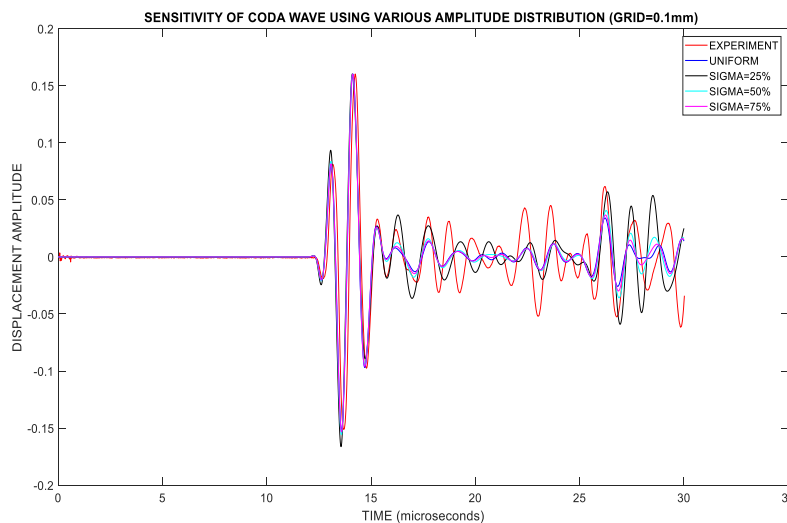


Figure 3: Measured (red) and model average displacement waveforms in AL sample using grid size of 0.1mm, for a source with uniform amplitude input (blue), and Gaussian distribution with $\sigma = 25\%$ (black), 50% (cyan), and 75% (magenta). The source central frequency=1MHz, and voltage= 100V.

In addition to that, a finer grid reduces the error misfit between the synthetic and the measured data. A peak value manually estimated as the maximum position of P-wave in the synthetic waveforms for two grid sizes displayed in Table 1. This measure is fairly stable for 0.45 mm grid size, while a deviation of about 0.1μs for 0.1 mm. Finer grid tend to correct the coda misfit, but alternatively, introduce a peak-to-peak displacement dispersion which could corrected using a suitable convergence criterion. Similar to the correction provided by higher σ , the same behaviour (small error) is observed for a finer grid. To obtain higher accuracy results similar to a uniform source, higher σ needs to be considered for a source with a Gaussian amplitude.

Table 1: Estimated maximum amplitude peak position for two different grid sizes (Measured peak reference=14.24μs,) for a source amplitude distributed uniformly (U) and non-uniformly with varying σ (sample: AL)

Input grid size(mm)	U(μs)	25%(μs)	50%(μs)	75%(μs)
0.45	14.2	14.2	14.2	14.22
0.1	14.1	14.1	14.11	14.13

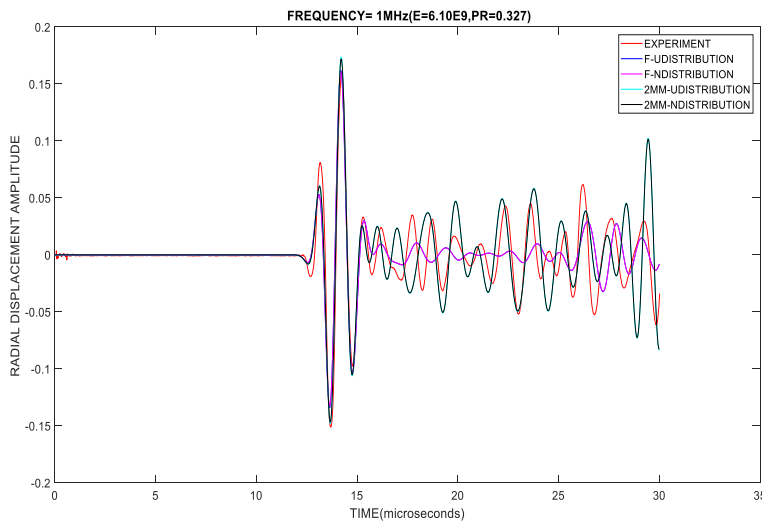


Figure 4: Measured (red) and model average displacement waveforms in AL sample using grid size of 0.45mm for a radial ($\approx 2mm$) (cyan and black) and linear (blue and magenta) source/receiver arrays are used. The source central frequency=1MHz, and voltage= 100V.

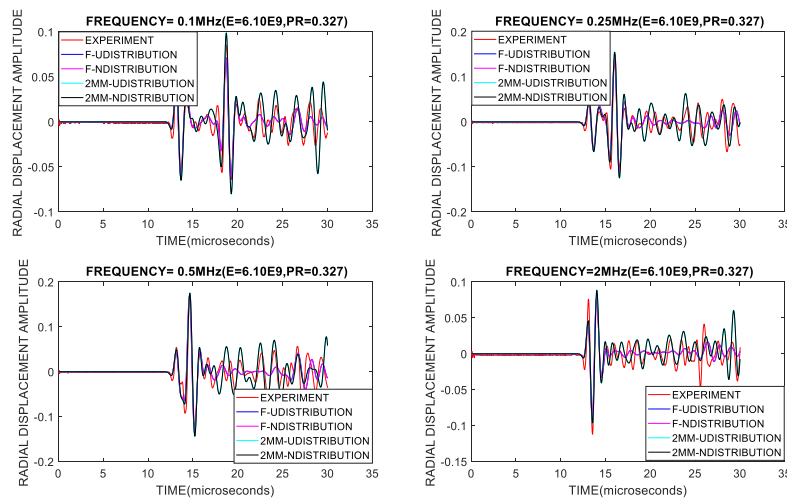


Figure 5: Same as in Figure 4, tlf=0.1MHz, trf=0.25MHz, blf=0.5MHz, brf=2MHz t:top, l:left, r:right, b:bottom f:frequency

To model the waveforms accurately, it is important to investigate the effect of the finite transducers sizes and signal distortion which might be caused by the contact between the transducer and the sample surface. However, for a simplified experiment conducted in this study, two model arrays such as radial ($\approx 2mm$) (Chen et. al., 2014) and linear (full receiver) are investigated. They can help to better analyse the misfit due to the geometrical configuration of the transducer arrays. In Figure 4, we show the measured data (red) and model average displacement waveforms for a radial (cyan and black) and linear (blue and magenta). Like in Figure 4, Figure 5 shows the results for various frequencies (0.1, 0.25, 0.5, 2 (MHz)). In these figures, the radial arrays fit the measured waveforms better than the linear array. However, the linear array error increases while its GOF decreases with the increasing frequencies. The error remains fairly constant for both uniform and distributed ($\sim 75\%$) amplitude input. Regardless of the low percentage error, the radial array visually matches the wave train better than the linear configuration.

Table 2: Estimated peak position of high amplitude peak in AL using various frequencies for radial, linear and measured data.

FREQ (MHz) \ Arrays	0.1	0.25	0.5	1.0	2-2.25
Radial (μs)	18.73	16	14.67	14.2	14.02
Linear(μs)	18.67	15.98	14.63	14.19	13.99
Measured(μs)	18.74	16.04	14.68	14.24	14.02

As described earlier, Table 2 shows estimated maximum peak position of high amplitude features of the synthetic waveforms using various frequencies (0.1, 0.25, 0.5, 1.0, 2-2.25 MHz) for radial, linear arrays and the experimental data. It shows high confidence for the radial array. The overall difference between the radial and measured arrays are about $0.01(\mu s)$, and $0.05(\mu s)$ for the linear array with the measured one. This error is small, and could be increase for a finer grid size of about $0.1mm$ as above.

Although E and v remain constant for both arrays, the parameters discussed above show a reasonable improvement of the displacement waveforms. The sample of AL in this work has a degree of heterogeneity which if taken into account could increase the accuracy of the waveforms fitting. With the assumption of a homogeneous and isotropic medium, it is not possible to accurately match the waveforms of a homogeneous medium such as AL77x38 using a P-wave transducer with a source input amplitude of two kinds. One way to reduce the error in the above modelling is to consider the inversion of the full waveform.

2. INVERSION MODELLING

The trivial initial inversion computation can be time-consuming and also very expensive because it involves many iterations of various forward models defined in the traditional grid search. However, a robust estimate of E and v that minimises the % diff between measured and synthetic data is obtained using the workflow in Figure 6. Our starting model parameters such as $E_0 = 65GPa$, $v_0 = 0.3$ with a step of $\Delta E_0 = 1GPa$ and $\Delta v_0 = 0.01$.

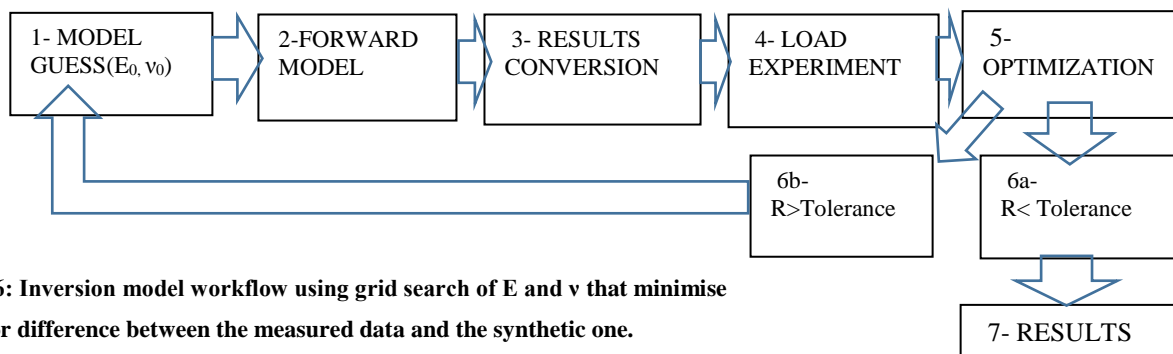


Figure 6: Inversion model workflow using grid search of E and v that minimise the error difference between the measured data and the synthetic one.

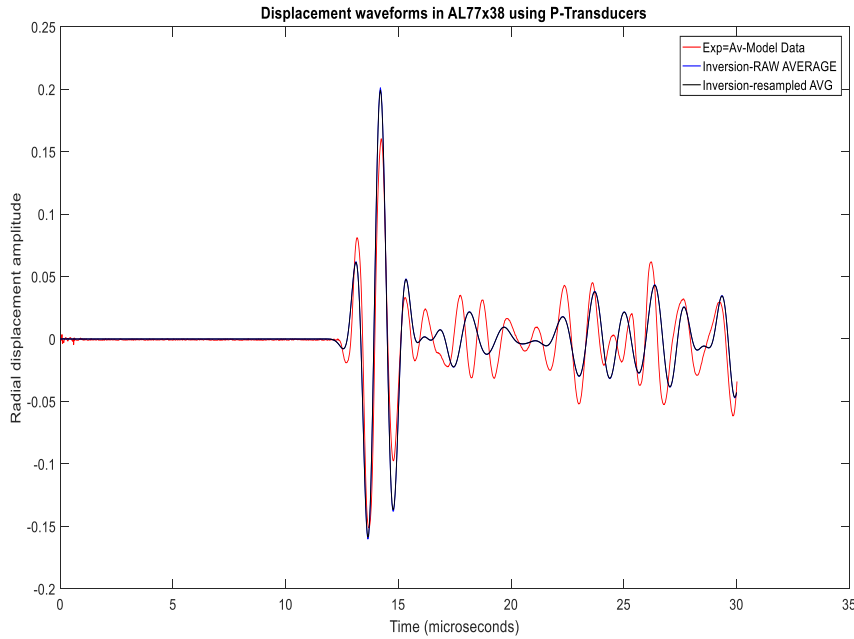


Figure 7: Inversion results of the axial displacement waveforms in AL sample using a radial array source and receivers with a uniform input. In blue (raw data) and black (average) is the synthetic data obtained iteratively for $E = 69\text{GPa}$, $\nu = 0.35$, and red the experimental data.

Figure 7 shows the synthetic (blue and black) waveforms resulted from our inversion compared with the measured data (red). Both blue and black curves are obtained using the same initial guesses ($E_0 = 65\text{GPa}$ and $\nu_0 = 0.3$). The waveforms match the measured data with a low error similar to the earlier described in Figure 4 (magenta and black curves). Our automated inversion algorithm does not depend on the quality of the initial parameters. However, if the first guess is randomly selected, the computational cost can increase largely. Besides that, our inversion will always converge to the minimized result difference. One way to reduce the computational cost is to use a method such as square global grid-search. Both forward and inversion modelling robustly estimates the elastic parameters that minimise the error between two waveforms, and their accuracy can depend on the source wave field. Because of inherent tradeoffs between parameters such as the normalisation coefficients of the average results prior to optimisation during the inversion, the results could suffer from longer computation cost. Our results do not suffer from the slight source-receiver shift but potentially suffer from non-uniqueness of the source-receiver array configuration.

3. CONCLUSIONS

The most important factors to reach a high precision of the displacement waveforms using both forward modelling and inversion are the accuracy of the source shape and its amplitude distribution. In this work, we modelled and validated a source input amplitude of two types: uniform and non-uniform distribution. Linear array configuration does not visually fit better with the waveforms compare to the radial configuration. This can be due to the following facts: a) there is more shots received, and those from far offsets which are broader can strongly affect the average displacement waveforms, b) the standard deviation of the source amplitude input is not accurate enough to correct the displacement waveforms of the far offset.

Introducing various source input amplitude distribution reduces the error in fitting the waveforms displacement. In a radial configuration, both inversion and forward model visually show a high correlation of the displacement waveforms. However, the linear array receiver shows the best statistical results with the best-constrained parameters E and ν which have a strong influence on the first break travel time. Also, with prior knowledge of P-wavelength, a finer mesh is required to fit even the coda waves robustly. This not only improves the displacement frequency dispersion but also the spatial resolution of the displacement even when the experiment is conducted below or above the nominal frequency of the P-wave transducer.

ACKNOWLEDGMENTS

The authors thank the sponsors of the Curtin Reservoir Geophysics Consortium (CRGC) for their financial support.

REFERENCES

- Alles, E. J., M. D. Verweij and K. W. A. Van Dongen, 2010, Reconstruction transducer surface motion by inverse extrapolation of measured pressure wavefields: IEEE International Ultrasonics Symposium Proceedings, 1458-1461.
- Akram J. and D.W. Eaton, 2016, A review and appraisal of arrival-time picking methods for downhole microseismic data: *Geophysics*, 81, 67-87.
- Cavuto, A., F. Sopranzetti, and G.M., Revel, 2003, Laser-Ultrasonics Wave Generation and Propagation FE Model in Metallic Materials: Excerpt from the Proceedings of 2013 COMSOL Conference in Rotterdam.
- Chen Y., Lam, K.H., Zhou D., Yue Q., Yu Y., Wu J., Qiu W., Sun L., Zhang C., Luo H., Chan H. L. W., and J. Dai, 2014, High performance relaxor-ferroelectric single crystals for ultrasonic transducers applications: *Sensors*, 14, 13730-13758.
- Daley, P. F., and F. Hron, 1977, Reflection and transmission coefficients for transversely isotropic media: *Bulletin of the Seismological Society of America*, 67, 661-675.
- Dellinger, J., and L. Vernik, 1994, Do travel times in pulse-transmission experiments yield anisotropic group or phase velocities? *Geophysics*, 59, 1774-1779.
- Kamath N., and I. Tsvankin, 2014, Elastic full-waveform inversion of transmission data in 2D VTI media: Centre for Wave Phenomena (CWP) reports-804, SEG.
- Lee, W. M., and W. F. Waite, 2009, High-frequency normal mode propagation in aluminum cylinders: Scientific investigators report 5142, USGS.
- Mikhaltsevitch, V., M. Lebedev, and B. Gurevich, 2014, A laboratory study of low-frequency wave dispersion and attenuation in water-saturated sandstones: The leading edge, special section: attenuation dispersion, 614-622.
- Olympus NDT, 2007, *Advances in Phased Array Ultrasonic Technology Applications*; Olympus NDT: Waltham, MA, USA.
- Qi, H., H. De-Hua and L. Hui, 2015, Laboratory measurement of dispersion and attenuation in the seismic frequency: SEG New Orleans, 3090-3094.
- Li R., P. Okoye and N. Uren, 2000, A study of the effect of the transducer size on physical modelling experiments for recovering anisotropic elastic parameters: *Geophys Research Letters*, 27, 3643-3646.
- Rasolofosaon, P. N. J., and B. E. Zinszner, 2014, *Petroacoustics - A tool for applied seismic*, Chapter 2 on "Laboratory measurements", EDP Sciences.
- Santamarina, J. A., Klein, K.A., and Fam, M.A., 2001, *Soils and Waves: Particulate materials behavior, characterization and process monitoring*: New York, Wiley, 488.
- Shin, C., D. Min, K. J. Marfurt, H. Lim, D. Yang, Y. Cha, S. Ko, K. Yoon, T. Ha and S. Hong, 2002, Traveltime and amplitude calculations using the damped wave solution: *Geophysics* 67, 1637-1647.
- Shragge, J., T. E. Blum, K. V. Wijk and A. Ludmila, 2015, Full-wavefield modelling and reverse time migration of laser ultrasound data: A feasibility study: *Geophysics*, 80, 553-563.
- Simons, J.A., Turner, C. D., and H. N. G. Wadley; 1987, Vector calibration of ultrasonic and acoustic emission transducers, *J. Acoust. Soc. Am.* 82 (4); 1122-1130.
- Yun, T.S., Narsilio, G.A., Santamarina, J.C., and Ruppel, C., 2006, Instrumented pressure testing chamber for characterizing sediment cores recovered at in situ hydrostatic pressure: *Marine Geology*, 229, 285-293.
- Waite, W.F., Kneafsey, T.J., Winters, W.J., and Mason, D.H., 2008, Physical property changes in hydrate-bearing sediment due to depressurization and subsequent repressurization: *Journal of Geophysical Research*, 113. B07102, doi:10.1029/2007JB005351.
- Waite, W.F., Winters, W.J., and Mason, D.H., 2004, Methane hydrate formation in partially water-saturated Ottawa sand: *American Mineralogist*, 89, p.1202-1207.
- Yoshimitsu, N., T. Furumura and T. Maeda, 2016, Geometric effect on a laboratory-scale wavefield inferred from a three-dimensional numerical simulation: *J. Appl. Geo.*, 132, 184-192.
- Zhang, Y., L. Y. Fu, L. Zhang, W. Wei and X. Guan, 2014, Finite difference modelling of ultrasonic propagation (coda waves) in digital porous cores with un-split convolutional PML and rotated staggered grid: *Journal of Applied Geophysics*, 104, 75-89.